

# An Atomistic Modeling Study of the Relationship between Critical Resolved Shear Stress and Atomic Structure Distortion in FCC High Entropy Alloys — Relationship in Random Solid Solution and Chemical-Short-Range-Order Alloys —

Md. Lokman Ali<sup>1,2,\*</sup>, Shuhei Shinzato<sup>1</sup>, Vei Wang<sup>3</sup>, Zeqi Shen<sup>1</sup>, Jun-ping Du<sup>1,4</sup> and Shigenobu Ogata<sup>1,4</sup>

<sup>1</sup>Department of Mechanical Science and Bioengineering, Graduate School of Engineering Science, Osaka University, Toyonaka 560-8531, Japan

<sup>2</sup>Department of Physics, Pabna University of Science and Technology, Pabna-6600, Bangladesh

<sup>3</sup>Department of Applied Physics, Xi'an University of Technology, Xi'an 710054, China

<sup>4</sup>Center for the Element Strategy Initiative for Structural Materials (ESISM), Kyoto University, Kyoto 606-8501, Japan

The relationship between the critical resolved shear stress (CRSS) at  $T = 0$  K and the atomic structure distortion was studied using molecular dynamics (MD) simulation with atomic distortion (root-mean-square-atomic-displacement (RMSAD)) controlled Lennard-Jones (LJ) interatomic potentials for different face-centered-cubic (FCC) high entropy alloy (HEA) systems, such as ternary, quaternary, and quinary alloy systems. We demonstrated that an almost universal linear relationship exists between CRSS and RMSAD for the random solid solution (RSS) of these alloy systems. The universality was also confirmed by a more realistic embedded atom method (EAM) potential. However, alloy systems that have a chemical-short-range-order (CSRO) do not follow this universal linear relationship. [doi:10.2320/matertrans.MT-MK2019007]

(Received January 9, 2020; Accepted January 23, 2020; Published March 25, 2020)

**Keywords:** molecular dynamics, high entropy alloy, critical resolved shear stress, root-mean-square-atomic-displacement, Lennard-Jones potential, chemical-short-range-order

## 1. Introduction

High entropy alloys (HEAs) are almost random solid solution (RSS) alloys comprising of five or more metallic elements with equiatomic or nearly equiatomic proportion. HEAs have attracted tremendous attention from the materials science research community due to their remarkable mechanical properties when applied as a structural material. This properties include excellent cryogenic temperature ductility,<sup>1)</sup> high mechanical strength,<sup>2,3)</sup> good wear resistance,<sup>4)</sup> exceptional damage tolerance,<sup>1,5,6)</sup> moderate strain-rate sensitivity,<sup>2)</sup> and high thermal stability.<sup>4,7)</sup> The design and development of a new HEA that has better mechanical properties than the presently existing HEAs have been a major challenge. Recently, a universal linear relation between the critical resolved shear stress (CRSS) and several atomic distortion parameters, like the root-mean-square-atomic-displacement (RMSAD),<sup>8)</sup> the atomic volume difference,<sup>9-11)</sup> and the local atomic strain,<sup>12)</sup> has been proposed and backed by experimental findings. Our first goal here is to demonstrate the universal relationship between CRSS and RMSAD in the ternary, quaternary, and quinary alloy systems using molecular dynamic (MD) simulations with emphasis on direct atomistic deformation testing. To achieve this goal, we developed RMSAD controlled Lennard-Jones (LJ) potentials for these alloy systems and performed direct dislocation glide analysis using these potentials. Another goal was to investigate the chemical-short-range-order (CSRO) effect on the universal linear relation. The existence of the CSRO in HEA has been strongly suggested in recent modeling<sup>13)</sup> and experimental studies.<sup>14,15)</sup> It is not surprising that there are atomic bonding preferences in such multi-element systems, which should lead to a local atomic ordering at low

temperatures where the effect of configurational entropy is expected to be lower than the effect of enthalpy.

## 2. Computational Methods and Models

### 2.1 Interatomic potential model

The LJ potential is simple and useful in qualitatively studying the movement of defects, such as dislocation glide, in metallic systems. Although the many-body effect was ignored in the interatomic interaction, the LJ potential was used in this work due to its flexibility in adjusting the RMSAD and making the CSRO in the HEA model. This flexibility enables the demonstration of the universal relation between CRSS, RMSAD, and CSRO effect on it. The LJ potential between the same element,  $i$ , is given by

$$U_{LJ} = 4\varepsilon_{ii} \left\{ \left( \frac{\sigma_{ii}}{r} \right)^{12} - \left( \frac{\sigma_{ii}}{r} \right)^6 \right\}, \quad (1)$$

where  $\varepsilon_{ii}$  is the depth of the energy well and  $\sigma_{ii}$  defines the cut-off distance of the interatomic interaction. The LJ potential for the elements  $i$  and  $j$  was determined using eq. (1). The potential parameters,  $\varepsilon_{ij}$  and  $\sigma_{ij}$ , are given by  $\varepsilon_{ij} = \sqrt{\varepsilon_{ii}\varepsilon_{jj}}$  and  $\sigma_{ij} = \sqrt{\sigma_{ii}\sigma_{jj}}$ . In this study, the Large-scale Atomic/Molecular Massively Parallel Simulator (LAMMPS)<sup>16)</sup> was used to perform for the MD simulations.

### 2.2 RMSAD computation method

The MD simulations were performed to determine the RMSAD values for different equiatomic alloying systems (ternary, quaternary and quinary) in a three-dimensional FCC crystal structure. The three-dimensional FCC crystal comprised of  $\sim 54,000$  atoms with a  $7.7 \times 8.9 \times 9.4$  nm<sup>3</sup> supercell under periodic boundary conditions in all three directions, such as (111), (1 $\bar{1}$ 0), and (11 $\bar{2}$ ) (See Fig. 1 for typical supercell). The specific number of atoms for all the

\*Corresponding author, E-mail: m.l.ali@tsme.me.osaka-u.ac.jp

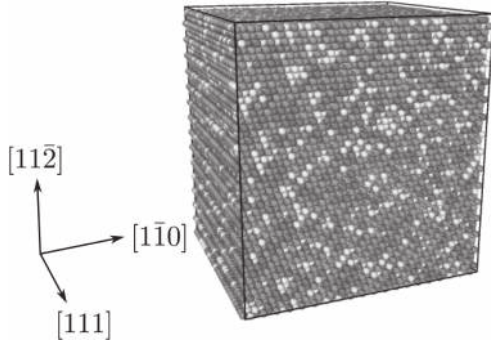


Fig. 1 Schematic representation of the simulated supercell.

elements were randomly arranged on the FCC lattice. The RMSAD of the LJ alloy systems was computed by the following procedure. First, (a) the volumetric supercell relaxation without atomic structure relaxation was performed on the model using NTP ensemble to keep the number of atoms ( $N$ ), temperature ( $T$ ) and pressure ( $P$ ) constant. Then, (b) atomic structure relaxation without supercell shape relaxation was performed to obtain a distorted atomic structure that deviated from the FCC lattice. The RMSAD values were computed from the atomic displacement that resulted during the atomic structure relaxation process (b) using the following equation:

$$\begin{aligned} \text{RMSAD} &\equiv \sqrt{\langle \Delta r^2 \rangle} = \sqrt{\frac{1}{N} \sum_{i=1}^N |r_i^{(\text{Relax})} - r_i^{(\text{Onlattice})}|^2} \\ &= \sqrt{\langle |r_i^{(\text{Relax})} - r_i^{(\text{Onlattice})}|^2 \rangle}, \end{aligned} \quad (2)$$

where  $r_i^{(\text{Relax})}$  is the atomic positions of atom  $i$  at the relaxed configuration and  $r_i^{(\text{Onlattice})}$  is the atomic positions of atom  $i$  on the FCC lattice configuration in the process (b),  $N$  is the total number of the atoms in the supercell. We chose the potential parameters that can model various alloys having different RMSADs. The potential parameters used for the ternary, quaternary, quinary alloy systems with various RMSADs are listed in Tables 1–3. The parameters  $\varepsilon_{ij}$  were set to 0.2 eV.

### 2.3 CSRO structure modeling method

To obtain a CSRO structure, we modified the LJ potential

Table 1 LJ parameters for ternary systems with corresponding mean-square-atomic-displacement (MSAD) values. The average Burgers vector  $b$  is computed from the supercell size after the volumetric relaxation.

RMSAD (Å)	$b$ (Å)	$\sigma_{11}$ (Å)	$\sigma_{22}$ (Å)	$\sigma_{33}$ (Å)
0.0501	2.356	2.24	2.12	2.10
0.0710	2.500	2.38	2.30	2.16
0.0876	2.568	2.48	2.28	2.26
0.104	2.423	2.36	2.14	2.11
0.111	2.477	2.36	2.32	2.06
0.123	2.344	2.30	2.06	2.02
0.134	2.344	2.32	2.04	2.00

Table 2 LJ parameters for quaternary systems with corresponding MSAD values. The average Burgers vector  $b$  is computed from the supercell size after the volumetric relaxation.

RMSAD (Å)	$b$ (Å)	$\sigma_{11}$ (Å)	$\sigma_{22}$ (Å)	$\sigma_{33}$ (Å)	$\sigma_{44}$ (Å)
0.0557	2.496	2.36	2.34	2.24	2.18
0.0657	2.508	2.42	2.28	2.24	2.22
0.0740	2.484	2.40	2.28	2.22	2.16
0.0815	2.469	2.40	2.26	2.18	2.17
0.0878	2.493	2.42	2.30	2.22	2.14
0.0983	2.467	2.42	2.24	2.18	2.14
0.111	2.438	2.40	2.22	2.16	2.08

parameter  $\varepsilon_{ij}$  for the quinary system in order to model a strong atomic bond between type 1 and type 2 atoms, this resulted in a CSRO structure with higher a bonding probability between them. The parameters of the modified LJ potential are shown in Table 4. A Monte Carlo (MC) annealing simulation at  $T = 0.83$  ( $1/T_m$ ,  $T_m$  is melting temperature) was performed by swapping the atomic positions. Figure 2 shows the energy reduction during the MC simulation and change in the CSRO parameters (Warren-

Table 3 LJ parameters for quinary systems with corresponding MSAD values. The average Burgers vector  $b$  is computed from the supercell size after the volumetric relaxation.

RMSAD (Å)	$b$ (Å)	$\sigma_{11}$ (Å)	$\sigma_{22}$ (Å)	$\sigma_{33}$ (Å)	$\sigma_{44}$ (Å)	$\sigma_{55}$ (Å)
0.0682	2.491	2.38	2.36	2.26	2.22	2.14
0.0840	2.512	2.42	2.40	2.24	2.20	2.18
0.0938	2.521	2.42	2.38	2.36	2.16	2.14
0.101	2.509	2.44	2.36	2.32	2.16	2.12
0.115	2.477	2.42	2.38	2.18	2.14	2.12
0.131	2.498	2.44	2.42	2.20	2.14	2.12
0.139	2.491	2.44	2.42	2.16	2.14	2.12

Table 4 LJ parameters for the quinary alloy considering CSRO. The average Burgers vector  $b$  is computed from the supercell size after the volumetric relaxation.

Parameter	Value	Parameter	Value
$\epsilon_{11}$ (eV)	0.4	$\sigma_{11}$ (Å)	2.336
$\epsilon_{22}$ (eV)	0.5	$\sigma_{22}$ (Å)	2.284
$\epsilon_{33}$ (eV)	0.5	$\sigma_{33}$ (Å)	2.319
$\epsilon_{44}$ (eV)	0.4	$\sigma_{44}$ (Å)	2.440
$\epsilon_{55}$ (eV)	0.5	$\sigma_{55}$ (Å)	2.281
$\epsilon_{12}$ (eV)	0.6	$\sigma_{12}$ (Å)	2.310

Cowley parameters<sup>17,18</sup>), that clearly demonstrate that the CSRO parameters deviate from zero which means that certain CSRO was formed in the model made by the MC simulation. The RMSAD value of this model is computed as 0.053 Å.

## 2.4 CRSS computation

The simulation supercell used for CRSS computation is depicted in Fig. 3, which consists of the FCC HEA structures (the random and the CSRO structures) along  $x = [1\bar{1}0]$ ,  $y = [11\bar{2}]$  and  $z = [111]$  with a size of  $50.9 \times 21.2 \times 9.8 \text{ nm}^3$  comprising of  $\sim 920,000$  atoms. One edge dislocation was inserted on the  $[111]$  plane. The periodic boundary conditions were applied in the  $x$  and the  $y$  directions, and free surface boundary condition was applied in the  $z$ -direction. The MD simulation supercell and atomic structure were fully relaxed at pressure,  $P = 0 \text{ Pa}$  in the  $x$  and  $y$  directions and at temperature,  $T \sim 0 \text{ K}$ . The three atomic layers on both the upper and the lower boundaries were treated as rigid bodies, and then shear strain was applied by applying incremental relative displacement of 0.005 nm on the upper rigid body to the lower body. The atomic structure was relaxed using the conjugate gradient method with a force tolerance of  $0.001 \text{ eV/\AA}$  after each incremental relative displacement. The applied shear stress is estimated from the

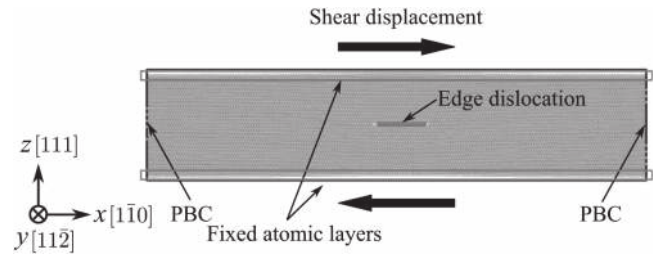


Fig. 3 Schematic illustration of the simulated supercell with one edge dislocation and the applied boundary conditions.

reaction force acting on the rigid shifting body over the cross-sectional area of the model in the  $\langle 111 \rangle$  direction. The CRSS is estimated as the shear stress acting when the dislocation starts to glide. In the CRSS computation, for each case we took an average of at least five CRSSs computed using five different atomic structures with the same energy and CSRO (randomness) level.

## 3. Results and Discussions

### 3.1 CRSS vs RMSAD

Figure 4 shows the relationship between the computed CRSS and RMSAD of the examined RSS alloys. For a fair comparison, each of the CRSS was normalized by the shear modulus of the model, and each RMSAD was normalized by average Burgers vector length. The relationship between the CRSS and the RMSAD for all the RSS alloy models were linear. The higher the RMSAD of the alloy, the higher the CRSS, regardless of the system being a ternary, quaternary, or quinary alloys. Note that the slope tends to decrease with increasing the number of elements. The fact maybe because of the spatial overlap between potential wells of the dislocation motion induced by the lattice distortion, which becomes more significant in the HEA having a larger number of different elements. The overlap should then lead to a milder relief in the fused potential landscape consists of the potential wells. To further confirm the universality of the linear relation, we also plotted the CRSS with existing embedded atom method (EAM) potential.<sup>19,20</sup> We found these data also followed a linear relation. However, the CRSS

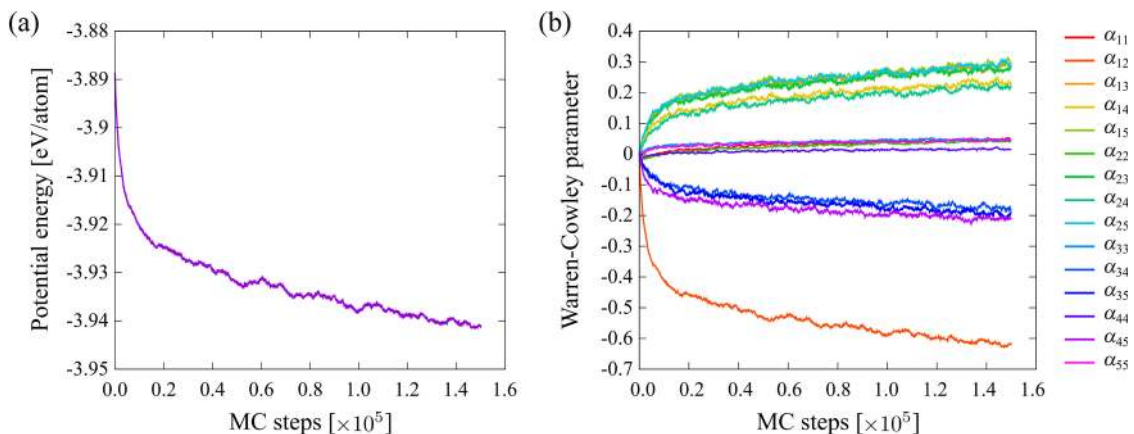


Fig. 2 (a) Energy reduction and (b) the change in the Warren–Cowley CSRO parameter ( $\alpha_{ij}$ ) observed during MC simulation. The indices  $i$  and  $j$  are atomic species.

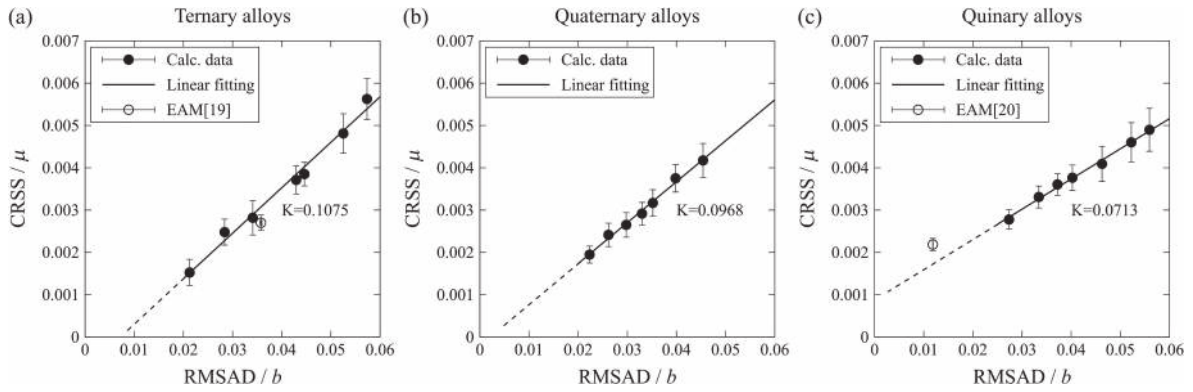


Fig. 4 Correlation between RMSAD and CRSS for (a) ternary, (b) quaternary, and (c) quinary FCC RSS alloys. The error bars indicate standard error.

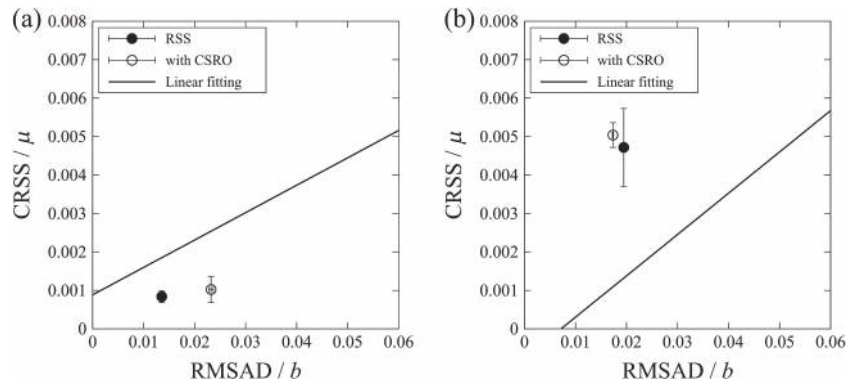


Fig. 5 Correlation between RMSAD and CRSS for alloys with and without CSRO using (a) modified LJ potential and (b) EAM potential.<sup>13)</sup> The solid line is the linear correlation of RSS alloys shown in Fig. 4. The error bars indicate standard error.

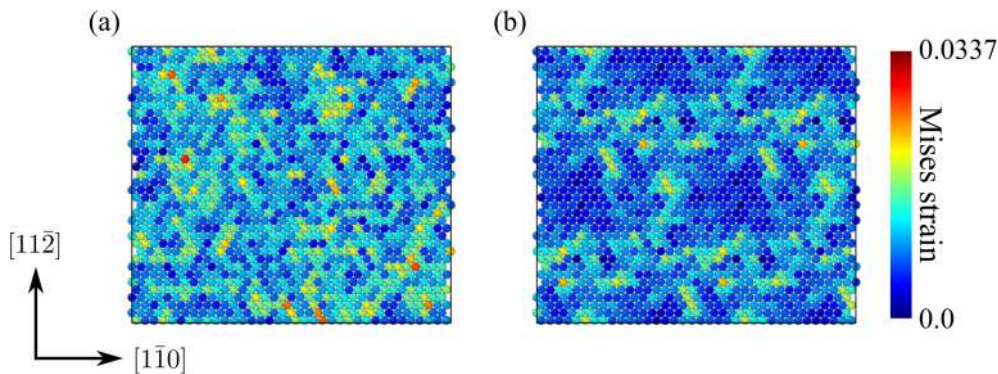


Fig. 6 Local atomic Mises strain distribution on [111] glide plane for alloys (a) without and (b) with CSRO. On-lattice atomic configuration after supercell volumetric relaxation was taken as the reference configuration of the atomic strain.

relationship for the RSS alloy (before MC relaxation) and the alloy with CSRO (after MC relaxation) alloy systems does not generally follow the linear relation as seen in Fig. 5. The quinary LJ alloys have almost the same CRSS even have quite different RMSADs. The EAM alloys<sup>13)</sup> show the totally opposite trend. Figure 6 shows local Mises atomic strain distribution<sup>21)</sup> in the RSS alloys and the alloy with CSRO. The alloy with CSRO mostly had lower atomic strain than the alloys without CSRO. The alloy with CSRO had a mesoscale pattern of a localized higher atomic strain region, suggesting that the atomic structure was stabilized by the formation of strong bonds between type 1 and type 2 atoms. It also

suggests the release of the average atomic strain, and thus the release of the atomic strain energy of the system. Meanwhile, the strong bonds formed between type 1 and type 2 atoms enabled the formation of the localized higher atomic strain region, and distorted the dislocation glide motion such as pinning effect, leading to the higher CRSS. Figure 7 shows the dislocation shape just before the glide motion for each alloy. The wavy and narrower dislocation core shape can be seen in the CSRO alloy, suggesting dislocation pinning resulted from the strong bond between the type 1 and type 2 atoms. Hence, to correctly predict the CRSS with CSRO, the in-glide-plane distribution of the local shear resistance or

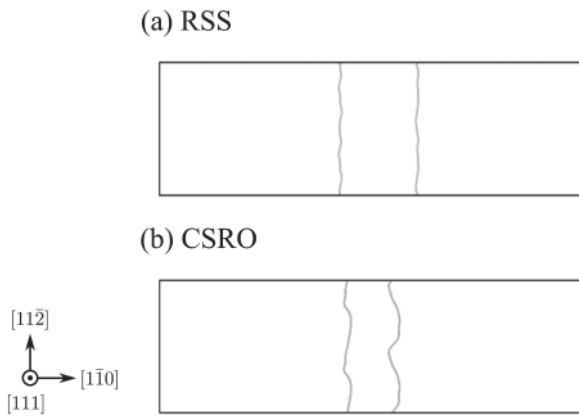


Fig. 7 Edge dislocation core structure under just below the critical shear stress for alloys (a) without and (b) with CSRO. Two partial dislocations of the edge dislocation core are visualized using a dislocation extraction algorithm (DXA).<sup>22)</sup>

stacking faults energies must be directly estimated rather than the volume average of geometrical distortion like the RMSAD, and then one may construct an in-glide-plane shear hardening model based on the distribution.

#### 4. Summary and Conclusion

In this paper, we have demonstrated that there exists a universal liner relationship between the CRSS and RMSAD (atomic distortion from FCC on-lattice). Using molecular dynamics simulations with RMSAD controlled LJ potentials, we were able to show that the higher RMSAD of the equiatomic ternary, quaternary, and quinary RSS alloys alloy, the higher CRSS. On the other hand, alloys with CSRO and alloys without CSRO do not follow the linear relation. This is because during the CSRO formation process, the atomic strain is released which reduces the total strain energy and thus changes the RMSAD, while a localized higher atomic strain region appeared. Meanwhile, strong bonds are formed which leads to a higher CRSS.

#### Acknowledgments

This work was supported by Element Strategy Initiative for Structural Materials (ESISM) of MEXT, Grant Number JPMXP0112101000. S.O. acknowledges the support by the JSPS KAKENHI Grant Nos. JP18H05450, JP18H05453, JP17H01238 and JP17K18827. S.S. acknowledges the support by the JSPS KAKENHI Grant No. JP19K23487.

#### REFERENCES

- 1) B. Gludovatz, A. Hohenwarther, D. Catoor, E. Cheng, E. George and R. Ritchie: *Science* **345** (2014) 1153.
- 2) A. Gali and E. George: *Intermetallics* **39** (2013) 74.
- 3) F. Otto, A. Dlouhy, C. Somsen, H. Bei, G. Eggeler and E. George: *Acta Mater.* **61** (2013) 5743.
- 4) M. Chuang, M. Tsai, W. Wang, S. Lin and L. Yeh: *Acta Mater.* **59** (2011) 6308.
- 5) Z. Zhang, M. Mao, J. Wang, B. Gludovatz, Z. Zhang, S. Mao, E. George, Q. Yu and R. Ritchie: *Nat. Commun.* **6** (2015) 10143.
- 6) Y. Zou, H. Ma and R. Spolenak: *Nat. Commun.* **6** (2015) 7748.
- 7) R. Sriharitha, B. Murty and R. Kottada: *J. Alloy. Compd.* **583** (2014) 419.
- 8) N. Okamoto, K. Yuge, K. Tanaka, H. Inui and E. George: *AIP Adv.* **6** (2016) 125008.
- 9) I. Toda-Caraballo and P. Rivera-Diaz-del-Castillo: *Acta Mater.* **85** (2015) 14.
- 10) I. Toda-Caraballo, E. Galindo-Nava and P. Rivera-Diaz-del-Castillo: *Acta Mater.* **75** (2014) 287.
- 11) Y. Zhao and T. Nieh: *Intermetallics* **86** (2017) 45.
- 12) Y. Ye, C. Liu, H. Wang and T. Nieh: *Acta Mater.* **147** (2018) 78.
- 13) Q.-J. Li, H. Sheng and E. Ma: *Nat. Commun.* **10** (2019) 3563.
- 14) J. Ding, Q. Yu, M. Asta and R. Ritchie: *Proc. Natl. Acad. Sci. USA* **115** (2018) 8919.
- 15) F. Zhang, S. Zhao, K. Jin, H. Xue, G. Velisa, H. Bei, R. Huang, J. Ko, D. Pagan, J. Neuefeind, W. Weber and Y. Zhang: *Phys. Rev. Lett.* **118** (2017) 205501.
- 16) S. Plimpton: *J. Comput. Phys.* **117** (1995) 1.
- 17) J. Cowley: *Phys. Rev.* **77** (1950) 669.
- 18) B. Warren: *X-Ray Diffraction*, (Dover Publications, New York, 1990).
- 19) G. Bonny, R. Pasianot, N. Castin and L. Malerba: *Philos. Mag.* **89** (2009) 3531.
- 20) D. Farkas and A. Caro: *J. Mater. Res.* **33** (2018) 3218.
- 21) F. Shimizu, S. Ogata and J. Li: *Mater. Trans.* **48** (2007) 2923.
- 22) A. Stukowski, V. Bulatov and A. Arsenlis: *Model. Simul. Mater. Sci. Eng.* **20** (2012) 085007.